Adaptive Output Force Tracking Control of Hydraulic Cylinders

Wen-Hong Zhu
Canadian Space Agency
6767 route de l'Aéroport
Saint-Hubert, QC J3Y 8Y9,
Canada
Wen-Hong.Zhu@space.gc.ca

Erick Dupuis
Canadian Space Agency
6767 route de l'Aéroport
Saint-Hubert, QC J3Y 8Y9,
Canada
Erick.Dupuis@space.gc.ca

Jean-Claude Piedboeuf
Canadian Space Agency
6767 route de l'Aéroport
Saint-Hubert, QC J3Y 8Y9,
Canada
Jean-Claude.Piedboeuf@space.gc.ca

***Abstract*— With respect to the output force control problem of the hydraulic cylinders, an adaptive control scheme is proposed by using direct output force measurements through loadcells. Due to the large and somewhat uncertain piston friction force, cylinder chamber pressure control with Coulomb-viscous friction compensation may not be sufficient enough to achieve a precise output force control. In the proposed approach, the output force error resulting from direct measurement is used to update the parameters of a novel friction model which includes not only the Coulomb-viscous friction force in sliding motion, but also the output force dependent friction force in presliding motion. The experimental results achieved on a hydraulic setup comprised of two hydraulic cylinders in pull-pull configuration demonstrate a frequency response of $\pm$1dB up to 20Hz. The excellent output force (joint torque) control performance implies the dynamic equivalency between the hydraulic actuation and the electrical actuation up to $10 \sim 20$Hz.**

I. INTRODUCTION

Hydraulic actuation has been widely used in industrial applications due to its high force to mass ratio. While this feature dramatically increases the operational capability of a hydraulic driven robot, the inherent nonlinearity associated with hydraulic cylinders heavily challenges the controller design. So far, most industrial hydraulic robots are still using PD position control. Enormous researches have been performed intending to apply advanced control approaches such as nonlinear feedback control and model based adaptive motion control into hydraulic cylinders aiming at significantly improving motion (position or velocity) tracking performance. However, the derived control laws are much more complicated than those derived for electrically-driven motors due to the specific dynamics of the hydraulic cylinders.

One solution to this challenge is to control the output force of the hydraulic cylinders and to establish dynamic equivalency between the hydraulic cylinders and the electrically-driven motors. Once the actual output force of a hydraulic cylinder tracks the desired force within a certain bandwidth, a hydraulic actuator can be viewed as dynamically equivalent to an electrical motor with the same force/torque control bandwidth. Thus, many motion/force control approaches previously developed for electrically-driven manipulators can be directly applied to hydraulic manipulators. This will allow cheap development of hydraulic control algorithms.

Some previous approaches intended to achieve force control by using chamber pressure control instead [1], [2]. A Coulomb-viscous friction model is usually incorporated to predict the cylinder output force. However, since the piston friction force is large and somewhat uncertain[1], calculating the cylinder output force based on a Coulomb-viscous friction model with fixed parameters may not be accurate enough. In this paper, a novel adaptive controller is proposed to control the cylinder output force. Loadcell sensors are used to directly measure the output force and the force error is used to update the parameters of a novel friction model which includes not only the Coulomb-viscous friction force in sliding motion, but also the output-force dependent friction force in presliding motion (when velocity is near zero).

This paper is organized as follows: in section II, a novel friction model is suggested. An adaptive control scheme which uses both output force and pressure measurements are presented in section III. In section IV, the experimental results are presented. Finally, it follows conclusion and references.

II. FRICTION MODEL

The piston friction makes a big difference between the output force and the chamber pressure force. A suitable friction model is necessary for achieving a good output force control performance.

A selective function $\mathcal{S}$ is designed as

$$\mathcal{S}(x) \triangleq \begin{cases} 1 & x(t) > 0 \\ 0 & x(t) \leq 0 \end{cases} \tag{1}$$

and a differentiable function $g(z, z_{ss})$ with a constant $z_{ss} > 0$ is defined as

$$g(z, z_{ss}) \triangleq \begin{cases} 1 & z \geq z_{ss} \\ z/z_{ss} & 0 < z < z_{ss} \\ 0 & z \leq 0 \end{cases} . \tag{2}$$

A Coulomb-viscous friction model with DC offset

$$\begin{aligned} f_c &= k_{cp} g(z, z_{ss}) \mathcal{S}(z) - k_{cn} g(-z, z_{ss}) \mathcal{S}(-z) + k_0 \\ &\quad + \left[k_{vp} \mathcal{S}(v) + k_{vn} \mathcal{S}(-v)\right] \phi(v) v \end{aligned} \tag{3}$$

[1]The experimental results suggest that the piston friction force amounts to thousands of Newton which is very much significant compared to the normal operational force (hundreds of Newton) required by most robotic tasks.

is used as part of the friction model devoted to sliding motion, where z denotes the average deformation of bristles [3, page 420] and $\dot{z}$ is governed by

$$\dot{z} = v - \frac{\mid v \mid}{z_{ss}} z \tag{4}$$

where v denotes the velocity. In (3), the first two terms in the right hand side devote to Coulomb friction and constant k_0 denotes a DC offset, and the last term in the right hand side devotes to the Stribeck and viscous friction with which $\phi(v)$ is an bounded and differentiable function characterizing the profile of the Stribeck and viscous friction. Parameters k_{cp} and k_{vp} correspond to positive v, and k_{cn} and k_{vn} correspond to negative v.

Remark 2.1: In this paper, the friction model (3) is mainly used in the sliding motion when $z = z_{ss}$ or $z = -z_{ss}$. Therefore, the damping term $\sigma_1 \dot{z}$ as suggested by [3] is not included.

Equation (3) describes the piston friction force in sliding motion. In presliding motion, it is found experimentally that the friction force is a function of the output force. The mathematical formulation can be expressed as

$$f_s = [k_{fp}\mathcal{S}(F) + k_{fn}\mathcal{S}(-F)]\,\varphi(F) \tag{5}$$

where F denotes the output force, and k_{fp} and k_{fn} are two positive constants associated with the positive and negative output force, respectively, and $\varphi(F)$ is a monotonic function defined as

1) $\varphi(0) = 0$
2) $\varphi(x) \geq \varphi(y)$ if $x \geq y$
3) $\mid \lim_{x \to \infty} \varphi(x) \mid \leq \gamma_{f1}$ with $0 < \gamma_{f1} < +\infty$
4) $\dot{\varphi}(x) = \gamma_{f2}(t)\dot{x}$ with $0 < \gamma_{f2}(t) < +\infty$.

One possible choice of $\varphi(F)$ is

$$\varphi(F) = \frac{F}{1 + \delta \mid F \mid} \tag{6}$$

with $\delta > 0$ be a constant.

Finally, the total piston friction force is represented as

$$f_f = [1 - \mathcal{L}(t)]f_c + \mathcal{L}(t)f_s \tag{7}$$

where $\mathcal{L}(t) \in [0, 1]$ is a differentiable function with $\mathcal{L}(t) \to 1$ for presliding motion and $\mathcal{L}(t) \to 0$ for sliding motion.

III. ADAPTIVE OUTPUT FORCE CONTROL

A. Cylinder Pressure Dynamics

Two cylinders in pull-pull configuration as illustrated in Figure 1 is studied in this paper.

The servovalves from TEXTRON have a spool position bandwidth of 200Hz. Therefore, it is reasonable to ignore the servovalve dynamics as performed in previous literatures [1], [4], i.e. the valve position is considered to be proportional to its control voltage.

Based on Bernoulli's static flow equation [5, page 41], the difference of flow speed squares at an orifice is proportional

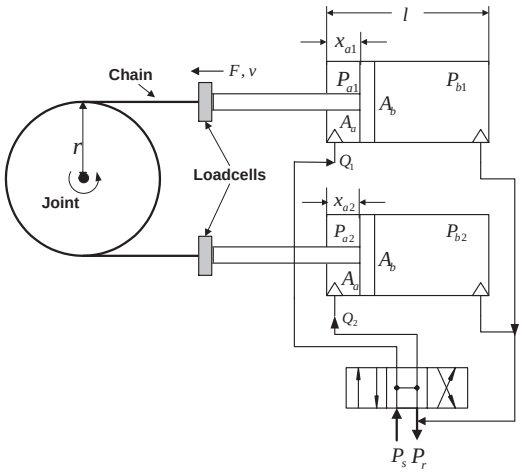

Fig. 1. Pull-pull configuration cylinders.

to the difference of pressures. As a result, the rate of flow passing through an orifice, denoted as Q^*, is proportional to a product of the valve control voltage and the root square of the pressure drop across the orifice, i.e.

$$Q^* = c\sqrt{\Delta P}u^* \tag{8}$$

where $c > 0$ is a constant, $\Delta P > 0$ denotes the pressure drop across the orifice, and u^* is the valve control voltage.

The dynamic equation of the fluid compressibility inside a chamber can be written as [1], [6]

$$\dot{P}^* = \frac{\beta}{V}(Q^* - \dot{V}) \tag{9}$$

where P^* denotes the chamber pressure, V denotes the chamber volume provided that the transmission line is thin enough with ignorable volume, Q^* is the rate of flow entering the chamber, and β is the fluid bulk modulus.

With the system as shown in Figure 1, it follows that $V_{a1} = A_a x_{a1}$ and $V_{a2} = A_a x_{a2}$, where V_{a1} and V_{a2} denote the chamber volumes of the two cylinders with A_a representing the piston area, and x_{a1} and x_{a2} denote the chamber displacements satisfying

$$x_{a1} = \frac{l}{2} + \delta_1 - r\psi \tag{10}$$

$$x_{a2} = \frac{l}{2} + \delta_2 + r\psi \tag{11}$$

where l is the length of the chamber, δ_1 and δ_2 are two constants representing the assembly offsets, ψ and r denote the rotational angle and the driving radius.

Let Q_1 and Q_2 be the rates of flow entering the upper and lower chambers, respectively, as shown in Figure 1. It

follows from (8) that

$$Q_1 = \begin{cases} c_{p1}\sqrt{P_s - P_{a1}}u^* & u^* > 0 \\ 0 & u^* = 0 \\ c_{n1}\sqrt{P_{a1} - P_r}u^* & u^* < 0 \end{cases} \quad (12)$$

$$Q_2 = \begin{cases} -c_{n2}\sqrt{P_{a2} - P_r}u^* & u^* > 0 \\ 0 & u^* = 0 \\ -c_{p2}\sqrt{P_s - P_{a2}}u^* & u^* < 0 \end{cases} \quad (13)$$

where P_s and P_r represent the supply and return pressures, P_{a1} and P_{a2} represent the pressures inside the upper and lower chambers, respectively, u^* is the valve control voltage, $c_{p1} > 0$ and $c_{n1} > 0$ are two constants associated with the flows entering and leaving the upper chamber, and $c_{p2} > 0$ and $c_{n2} > 0$ are two constants associated with the flows entering and leaving the lower chamber.

In view of (9), the pressure equations of the two chambers are written as

$$\dot{P}_{a1} = \frac{\beta}{A_a x_{a1}}(Q_1 + A_a v) \quad (14)$$

$$\dot{P}_{a2} = \frac{\beta}{A_a x_{a2}}(Q_2 - A_a v) \quad (15)$$

where v is the linear velocity along the cylinders. Note that the pressures inside the two cylinders can be converted into the net pressure force as

$$P = A_a(P_{a2} - P_{a1}) \, . \quad (16)$$

Subtracting (14) from (15) and using (12), (13), and (16) yield

$$\dot{P} = \beta \left[u - A_a \chi(t) v\right] \quad (17)$$

where

$$u = \begin{cases} -\left(\frac{c_{p1}\sqrt{P_s - P_{a1}}}{x_{a1}} + \frac{c_{n2}\sqrt{P_{a2} - P_r}}{x_{a2}}\right)u^* & u^* > 0 \\ 0 & u^* = 0 \\ -\left(\frac{c_{n1}\sqrt{P_{a1} - P_r}}{x_{a1}} + \frac{c_{p2}\sqrt{P_s - P_{a2}}}{x_{a2}}\right)u^* & u^* < 0 \end{cases} \quad (18)$$

$$\chi(t) = \frac{1}{x_{a1}} + \frac{1}{x_{a2}} \quad (19)$$

Once

$$P_s > P_{a1} > P_r \quad (20)$$

$$P_s > P_{a2} > P_r \quad (21)$$

hold together with $x_{a1} > 0$ and $x_{a2} > 0$, (18) and (19) are analytical and (18) is invertible such that the valve control signal u^* can be calculated form u. Equation (17) represents the dynamics of the cylinder pressures. Only two parameters β and A_a are involved.

B. Adaptive Control and Stability Analysis

The output force equation can be written as

$$F = P - f_f \quad (22)$$

where f_f represents the piston friction force governed by (7).

The control u is designed in terms of the cylinder dynamic model (17) as

$$u = \hat{k}_1 \dot{P}_d + \hat{A}_a \chi(t) v + k_p(P_d - P) + k_f(F_d - F) \quad (23)$$

where $\hat{k}_1$ and $\hat{A}_a$ denotes the estimates of $1/\beta$ and A_a, respectively; $k_p > 0$ and $k_f > 0$ are two control gains; F_d denotes the desired output force (the input to the controller) with bounded derivative ($\dot{F}_d \in L_\infty$); and P_d denotes the desired pressure that is designed, in view of (22), as

$$P_d = F_d + \hat{f}_f \quad (24)$$

$$\hat{f}_f = \mathcal{Y}_f \hat{\theta}_f \quad (25)$$

with

$$\mathcal{Y}_f = [(1 - \mathcal{L}(t))g(z, z_{ss})\mathcal{S}(z), -(1 - \mathcal{L}(t))g(-z, z_{ss})\mathcal{S}(-z), (1 - \mathcal{L}(t)), \ (1 - \mathcal{L}(t))\mathcal{S}(v)\phi(v)v, (1 - \mathcal{L}(t))\mathcal{S}(-v)\phi(v)v, \mathcal{L}(t)\mathcal{S}(F_d)\varphi(F_d), \mathcal{L}(t)\mathcal{S}(-F_d)\varphi(F_d)] \in \mathbf{R}^{1\times 7} \quad (26)$$

$$\theta_f = [k_{cp}, \ k_{cn}, \ k_0, \ k_{vp}, \ k_{vn}, \ k_{fp}, \ k_{fn}]^T \in \mathbf{R}^7 \quad (27)$$

where $\hat{\theta}_f$ denotes the estimate of θ_f. By using the $\mathcal{P}$ function defined in [7, page 311], the estimated parameters in (23)-(25) are updated by

$$\dot{\hat{k}}_1 = \mathcal{P}((P_d - P)\dot{P}_d, \rho_1, k_1^-, k_1^+) \quad (28)$$

$$\dot{\hat{A}}_a = \mathcal{P}((P_d - P)\chi(t)v, \rho_a, A_a^-, A_a^+) \quad (29)$$

$$(\dot{\hat{\theta}}_f)_i = \mathcal{P}((F_d - F)(\mathcal{Y}_f)_i, c_i, (\theta_f)_i^-, (\theta_f)_i^+), \quad i = 1, 2, \cdots, 7 \quad (30)$$

where $(\bullet)_i$ denotes the ith element of matrix/vector $\bullet$; $\rho_1 > 0$, $\rho_a > 0$, and $c_i > 0$ denotes the parameter updating gains; and $\bullet^-$ and $\bullet^+$ denote the lower and upper bounds of parameter $\bullet$, respectively.

An non-negative function is defined as

$$W = \frac{1}{2}\left\{\frac{1}{\beta}(P_d - P)^2 + \frac{1}{\rho_1}\left(\frac{1}{\beta} - \hat{k}_1\right)^2 + \frac{1}{\rho_a}(A_a - \hat{A}_a)^2 + \sum_{i=1}^{7}\frac{k_f}{c_i}\left[(\theta_f)_i - (\hat{\theta}_f)_i\right]^2\right\} \, . \quad (31)$$

In view of (17)-(25), (3), (5), (7), the time derivative of (31) can be written as

$$\begin{aligned} \dot{W} = & -k_p(P_d - P)^2 - k_f(F_d - F)^2 \\ & -k_f(F_d - F)\mathcal{L}(t)\left\{\left[\mathcal{S}(F_d)\varphi(F_d) - \mathcal{S}(F)\varphi(F)\right]k_{fp} \right. \\ & \left. + \left[\mathcal{S}(-F_d)\varphi(F_d) - \mathcal{S}(-F)\varphi(F)\right]k_{fn}\right\} \\ & + \left(\frac{1}{\beta} - \hat{k}_1\right)\left[(P_d - P)\dot{P}_d - \frac{1}{\rho_1}\dot{\hat{k}}_1\right] \\ & + (A_a - \hat{A}_a)\left[(P_d - P)\chi(t)v - \frac{1}{\rho_a}\dot{\hat{A}}_s\right] \\ & + \sum_{i=1}^{7}\left\{k_f[(\theta_f)_i - (\hat{\theta}_f)_i]\right. \end{aligned}$$

$$\left[(F_d - F)(\mathcal{Y}_f)_i - \frac{1}{c_i}(\dot{\hat{\theta}}_f)_i\right]\Bigg\} \ . \tag{32}$$

Based on the definitions of φ, $\mathcal{S}$ and $\mathcal{L}(t)$, it can be checked out that

$$\begin{aligned} &-k_f k_{fp}\mathcal{L}(t)(F_d - F)\left[\mathcal{S}(F_d)\varphi(F_d) - \mathcal{S}(F)\varphi(F)\right] \\ &\leq \ 0 \end{aligned} \tag{33}$$

$$\begin{aligned} &-k_f k_{fn}\mathcal{L}(t)(F_d - F)\left[\mathcal{S}(-F_d)\varphi(F_d) - \mathcal{S}(-F)\varphi(F)\right] \\ &\leq \ 0 \ . \end{aligned} \tag{34}$$

Furthermore, by using Lemma 1 in [7] (Equation (5) on page 311) together with (28)-(30), it follows that

$$\dot{W} \leq -k_p(P_d - P)^2 - k_f(F_d - F)^2 \ . \tag{35}$$

In view of (31) and (35), it yields

$$P_d - P \ \in \ L_\infty \cap L_2 \tag{36}$$

$$F_d - F \ \in \ L_2 \ . \tag{37}$$

Under bounded desired output force F_d and bounded velocity v (which can be ensured by using a stable motion controller such as the *virtual decomposition control* [7]), $\hat{f}_f$ is bounded in view of (25) and (26). This leads to bounded P_d in terms of (24). Consequently, pressure P is bounded in terms of (36), i.e.

$$\mid P \mid \leq \gamma_p < +\infty \ . \tag{38}$$

Meanwhile, the piston friction force f_f is also bounded in view of (3), (5), and (7). Therefore, the boundedness of the output force F is ensured from (22). Bounded output force implies bounded accelerations. Thus, under bounded $\dot{F}_d$, the boundedness of $\dot{P}_d$ can be ensured in terms of (24)-(27) and (30). Furthermore, $\dot{P}$ is bounded in view of (17) for bounded control u obtained from (23), i.e.

$$\mid \dot{P} \mid \leq \gamma_{pd} < +\infty \ . \tag{39}$$

Finally, the boundedness of $\dot{P}_d - \dot{P}$ is ensured such that $P_d - P$ is uniformly continuous. Based on [8], asymptotic stability of $P_d - P \to 0$ can be achieved. Since $\dot{P}$ is bounded and the derivative of f_f can be expressed as $\dot{f}_f = f_1(t) + f_2(t)\dot{F}$ with $\mid f_1(t) \mid \leq \gamma_f < +\infty$ and $f_2(t) > 0$, it follows that $\dot{F} = \dot{P} - \dot{f}_f \leq \dot{P} + \gamma_f - f_2(t)\dot{F}$ and furthermore $\dot{F} \leq (\dot{P} + \gamma_f)/(1 + f_2(t)) < +\infty$. The boundedness of $\dot{F}_d - \dot{F}$ implies that $F_d - F$ is uniformly continuous. Thus, asymptotic stability of $F_d - F \to 0$ is ensured from (37).

Below, the boundedness of all signals will be proven. define

$$\dot{P}^* = A_a(\dot{P}_{a2}x_{a2} + \dot{P}_{a1}x_{a1}) \ . \tag{40}$$

It follows from (12)-(15) that $\dot{P}^* = \mathcal{S}(u^*)\beta u^*(c_{p1}\sqrt{P_s - P_{a1}} - c_{n2}\sqrt{P_{a2} - P_r}) - \mathcal{S}(-u^*)\beta u^*(c_{p2}\sqrt{P_s - P_{a2}} - c_{n1}\sqrt{P_{a1} - P_r})$. Define $\Psi = \mathcal{S}(u^*)(c_{p1}\sqrt{P_s - P_{a1}} + c_{n2}\sqrt{P_{a2} - P_r}) + \mathcal{S}(-u^*)(c_{p2}\sqrt{P_s - P_{a2}} + c_{n1}\sqrt{P_{a1} - P_r}) > 0$. Multiplying Ψ to $\dot{P}^*$ yields $\Psi\dot{P}^* = \mathcal{S}(u^*)\beta u^*[c_{p1}^2(P_s - P_{a1}) - c_{n2}^2(P_{a2} - P_r)] - \mathcal{S}(-u^*)\beta u^*[c_{p2}^2(P_s - P_{a2}) - c_{n1}^2(P_{a1} - P_r)]$. When $P_r \approx 0$, this equation can be expressed as

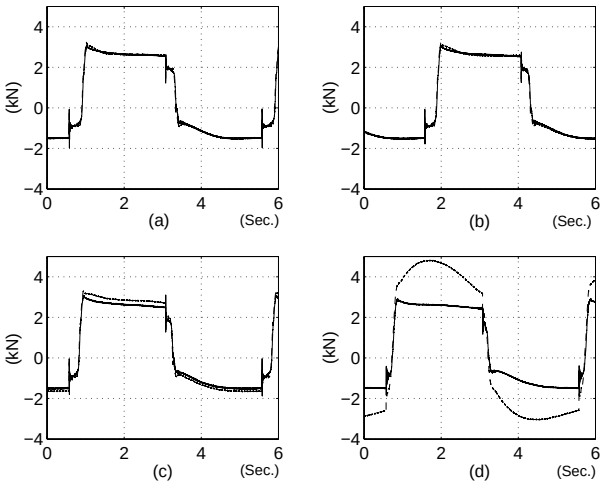

Fig. 2. Pressure tracking results between the desired pressure (force) P_d (dashed line) and the measured Pressure (force) P (solid line) with different cases of parameter adaptation for $\hat{A}_a$. Figures (a) and (b) correspond to $\rho_a = 700(V \cdot s/kN)$ and $\rho_a = 7(V \cdot s/kN)$, respectively, under $A_a^- = 6(V \cdot s)$ and $A_a^+ = 15(V \cdot s)$; figure (c) corresponds to $\hat{A}_a = (A_a^- + A_a^+)/2$ and figure (d) corresponds to $\hat{A}_a = 0$.

$$\dot{P}^* = \epsilon_1(t)P_s - \epsilon_2(t)P_{a1} - \epsilon_3(t)P_{a2} \tag{41}$$

with $\epsilon_1(t) > 0$, $\epsilon_2(t) > 0$, and $\epsilon_3(t) > 0$ subject to $\epsilon_1(t) < \epsilon_2(t) + \epsilon_3(t)$. In view of (16), adding both sides of (41) by $\dot{P}x_{a1}$ and replacing P_{a1} by $P_{a2} - \frac{P}{A_a}$ yield $(x_{a1} + x_{a2})A_a\dot{P}_{a2} = \epsilon_1(t)P_s - [\epsilon_2(t) + \epsilon_3(t)]P_{a2} + \epsilon_2(t)\frac{P}{A_a} + \dot{P}x_{a1}$. Since P and $\dot{P}$ are bounded and independent of P_s, see (38) and (39), once the supply pressure P_s is chosen as

$$P_s > \frac{A_a\gamma_{pd}\max\{x_{a1}, x_{a2}\} + \gamma_p\max\{\epsilon_2(t), \epsilon_3(t)\}}{A_a\min\{\epsilon_1(t), \epsilon_2(t) + \epsilon_3(t) - \epsilon_1(t)\}} \tag{42}$$

it follows that

$$\begin{aligned} &\dot{P}_{a2} > 0 \quad \text{if } P_{a2} = 0 \\ &\dot{P}_{a2} < 0 \quad \text{if } P_{a2} = P_s \ . \end{aligned} \tag{43}$$

Therefore, condition (21) will be valid $\forall t > 0$. Similarly, subtracting both sides of (41) by $\dot{P}x_{a2}$ and replacing P_{a2} by $P_{a1} + \frac{P}{A_a}$ yield $(x_{a1} + x - a2)A_a\dot{P}_{a1} = \epsilon_1(t)P_s - [\epsilon_2(t) + \epsilon_3(t)]P_{a1} - \epsilon_3(t)\frac{P}{A_a} - \dot{P}x_{a2}$. Under condition (42), it follows that

$$\begin{aligned} &\dot{P}_{a1} > 0 \quad \text{if } P_{a1} = 0 \\ &\dot{P}_{a1} < 0 \quad \text{if } P_{a1} = P_s \ . \end{aligned} \tag{44}$$

Thus, condition (20) will be valid $\forall t > 0$.

IV. EXPERIMENTS

In this section, experimental results will be demonstrated when the proposed adaptive output force controller is applied to the first joint of a six-joint hydraulic robot (STVF) installed at Canadian Space Agency [9].

An advanced computer control system running QNX based operating system RT-LAB from OPAL-RT with a

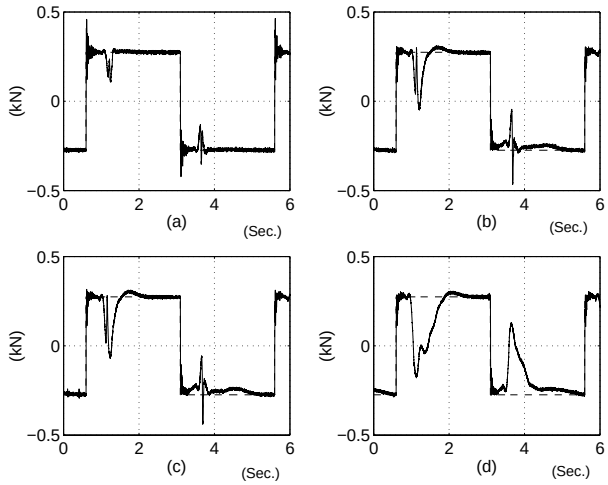

Fig. 3. Output force tracking results between the desired force F_d (dashed line) and the measured force F (solid line) with different cases of parameter adaptation for $\hat{k}_{cp}$ and $\hat{k}_{cn}$ under active $\hat{k}_0$. Figures (a) and (b) correspond to $c_1 = c_2 = 100(1/s)$ and $c_1 = c_2 = 1(1/s)$, respectively, with $c_3 = 20(1/s)$, under $k_{cp}^- = k_{cn}^- = 0$ and $k_{cp}^+ = k_{cn}^+ = 2.0(kN)$; figure (c) corresponds to $\hat{k}_{cp} = (k_{cp}^- + k_{cp}^+)/2 = 1.0(kN)$ and $\hat{k}_{cn} = (k_{cn}^- + k_{cn}^+)/2 = 1.0(kN)$, and figure (d) corresponds to $\hat{k}_{cp} = 0$ and $\hat{k}_{cn} = 0$.

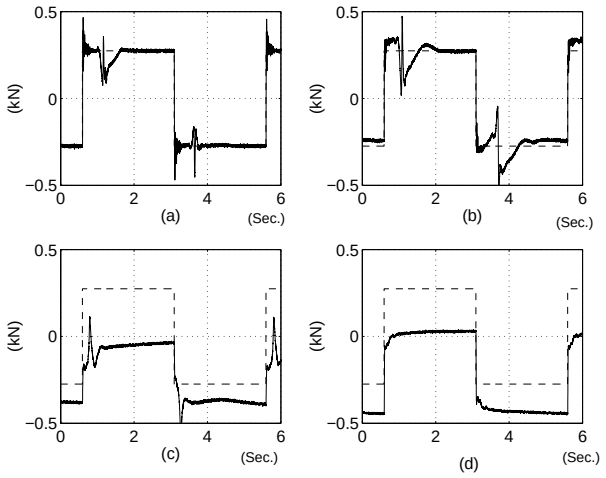

Fig. 4. Output force tracking results between the desired force F_d (dashed line) and the measured force F (solid line) with different cases of parameter adaptation for $\hat{k}_{cp}$ and $\hat{k}_{cn}$ under inactive $\hat{k}_0 = 0$. Figures (a) and (b) correspond to $c_1 = c_2 = 100(1/s)$ and $c_1 = c_2 = 1(1/s)$, respectively, under $k_{cp}^- = k_{cn}^- = 0$ and $k_{cp}^+ = k_{cn}^+ = 2.0(kN)$; figure (c) corresponds to $\hat{k}_{cp} = (k_{cp}^- + k_{cp}^+)/2 = 1.0(kN)$ and $\hat{k}_{cn} = (k_{cn}^- + k_{cn}^+)/2 = 1.0(kN)$, and figure (d) corresponds to $\hat{k}_{cp} = 0$ and $\hat{k}_{cn} = 0$.

multi-processor configuration is being used with a sampling rate of 1000Hz. The measurements include: the chamber pressures P_{a1}, P_{a2}, the supply pressure P_s, the loadcell force F, and the joint angle ψ read by using a 23-bit absolute encoder. The linear velocity v is derived from x_{a1}. The control output is the valve voltage u^*. Note that u in (23) is a virtual control variable. Therefore, in control implementation the unit of u^* (Volt) is used instead.

The function $\phi(v)$ in (3) is chosen as -1 to accommodate the Stribeck effect only, since the operational velocity of the robot is very low such that the velocities of the cylinders in most circumstances are limited by a range of $3cm/s$ which is dominated by Stribeck friction [1].

The function $\mathcal{L}(t)$ is basically a differentiable switching function that ensures a smooth transition between sliding motion and presliding motion. A design used in this paper is

$$\begin{aligned} \mathcal{L}(t) &= 1/[1 + (\delta_1 \tilde{v})^3] \\ \dot{\tilde{v}} &= 10(\mid v \mid -\tilde{v}) \end{aligned}$$

where $\delta_1 = 300(s/m)$ is a constant and $\tilde{v} \geq 0$ with $\tilde{v}(0) = 0$.

The feedback gains are $k_p = 1.2(V/kN)$ and $k_f = 2.4(V/kN)$, The pressure differential parameter $\hat{k}_1 = 0.01(V \cdot s/kN)$ is used as a constant.

A. Pressure Control

Figures 2 illustrates the pressure tracking results. The dashed lines represent the desired pressure P_d and the solid lines represent the measured pressure P. Figure 2 (a) shows the result of using (23) with a full version of parameter adaptation (29). Figure 2 (b) shows the result when the parameter adaptation gain ρ_a is reduced 100 times while keeping the other parameters unchanged. Figure 2 (c) shows the result when the parameter adaptation stops and a fixed parameter ($\hat{A}_a = 10(V \cdot s)$), which is the average of the lower and upper bounds, is used instead. Figure 2 (d) shows the result when there is no velocity compensation.

The experimental results demonstrate that the parameter adaptation gain has a weak impact on the pressure tracking control, since the difference between Figure 2 (a) and (b) is not significant. However, using parameter adaptation does produce a better result than using fixed parameters, the difference is reflected between Figure 2 (b) and (c). Finally, the pressure doesn't track at all if the velocity feedforward compensation is not added.

B. Output Force Control

Figures 3 and 4 demonstrate the experimental results of using different compensations with respect to the piston Coulomb friction. The dashed lines represent the desired output force F_d and the solid lines represent the actual output force F. Figure 3 (a) shows the output force tracking result with a full version of parameter adaptation (30). Figure 3 (b) shows the output force tracking result when the parameter adaptation gains c_1 and c_2 are reduced 100 times, while keeping the other parameters unchanged. Figure 3 (c) shows the output force tracking result when the parameter adaptation stops and a set of fixed parameters ($\hat{k}_{cp} = \hat{k}_{cn} = 1.0(kN)$) is used instead. Figure 3 (d) shows the output force tracking result when there is no Coulomb friction compensation (($\hat{k}_{cp} = \hat{k}_{cn} = 0$)). Figure 4 corresponds to Figure 3 except that $\hat{k}_0 = 0$ is used.

Both the Coulomb friction compensation characterized by

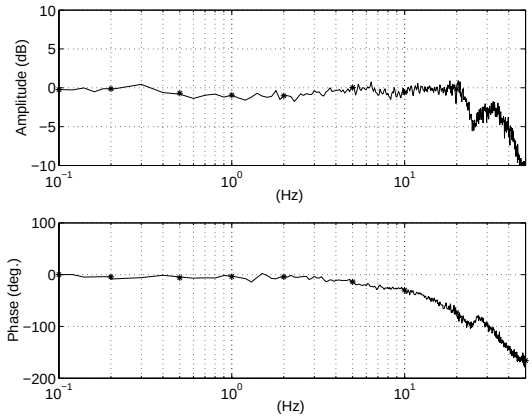

Fig. 5. Transfer function of output force tracking control.

$\hat{k}_{cp}$ and $\hat{k}_{cn}$ and the DC offset compensation characterized by $\hat{k}_0$ contribute to the output force tracking performance. By either disabling the DC offset compensation or reducing the parameter adaptation gains or disabling the parameter adaptation for Coulomb compensation, the output force tracking performance will be degraded. This can be clearly seen by observing the differences between Figure 3 (a) and Figure 4 (a) for disabling the DC offset compensation, between Figure 3 (a) and Figure 3 (b) for reducing the parameter adaptation gains, and between Figure 3 (a) and Figure 3 (c) for disabling the parameter adaptation for $\hat{k}_{cp}$ and $\hat{k}_{cn}$. The close observation between Figure 3 (b) and Figure 3 (c) indicates a small difference between low-gain parameter adaptation and fixed parameter compensation for $\hat{k}_{cp}$ and $\hat{k}_{cn}$ provided that the adaptation of the DC offset $\hat{k}_0$ is active. However, the difference will be big once $\hat{k}_0$ is inactive with $\hat{k}_0 = 0$, as shown in Figure 4 (b) and Figure 4 (c). The poor tracking performances in Figure 3 (d) and Figure 4 (d) correspond to no parameter compensation for $\hat{k}_{cp}$ and $\hat{k}_{cn}$.

Finally, the transfer function $20log_{10}(F/F_d)$ (dB) is shown in Figure 5, where $*$ indicates the frequency responses when individual sinusoidal excitations are added to the white noise excitation for improving the confidence of the transfer function. The transfer function demonstrates a 20Hz bandwidth within $\pm 1dB$.

V. CONCLUSION

In this paper, a novel adaptive control scheme is proposed to control the output force of the hydraulic cylinders. Unlike some previous approaches where only the chamber pressure is measured and controlled, and the output force is predicted by using a friction model with fixed parameters, the proposed controller directly measures the output force by using loadcells. The error between the desired output force and the measured output force is not only used for feedback control, but also used to update the parameters of a friction model which incorporates Coulomb, Stribeck, and viscous frictions in sliding motion and output-force dependent frictions in presliding motion. L_2 and L_∞ stability and furthermore asymptotic stability are guaranteed for both pressure control and output force control.

The experimental results have clearly demonstrated the necessity of using parameter adaptation to handle both the velocity based pressure compensation and the piston friction force compensation. Finally, the proposed output force controller demonstrated its ability to reach a bandwidth of 20Hz within $\pm 1dB$, which clearly indicates the dynamic equivalency between the hydraulic actuation and the electrical actuation in robotic applications.

REFERENCES

[1] G. A. Sohl and J. E. Bobrow, "Experiments and simulations on the nonlinear control of a hydraulic servosystem," *IEEE Trans. Control Systems Technology*, vol. 7, no. 2, pp. 238-247, 1999.

[2] A. Alleyne and R. Liu, "On the limitations of force tracking control of for hydraulic servosystems," *ASME J. Dynamic Systems, Measurement, and Control*, vol. 121, no. 2, pp. 184-190, 1999.

[3] C. Canudas de Wit, H. Olsson, K. J. Astrom, and P. Lischinsky, "A new model for control of systems with friction," *IEEE Trans. Automatic Control*, vol. 40, no. 3, pp. 419-425, 1995.

[4] B. Yao, F. Bu, and J. Reedy, and G. T.-C. Chiu, "Adaptive robust motion control of single-rod hydraulic actuators: theory and experiments," *IEEE/ASME Trans. Mechatronics*, vol. 5, no. 1, pp. 79-91, 2000.

[5] H. E. Merrit, *Hydraulic Control Systems*, New York: Wiley, 1976.

[6] M. R. Sirouspour and S. E. Salcudean, "Nonlinear control of hydraulic robots," *IEEE Trans. Robotics and Automation*, vol. 17, no. 2, pp. 173-182, 2001.

[7] W. H. Zhu and J. De Schutter, "Adaptive control of mixed rigid/flexible joint robot manipulators based on virtual decomposition," *IEEE Trans. Robotics and Automation*, vol. RA-15, no. 2, pp. 310-317, 1999.

[8] G. Tao, "A simple alternative to the Barbălat lemma," *IEEE Trans. Automatic Control*, vol. 42, no. 5, p. 698, 1997.

[9] J.-C. Piedboeuf, J. de Carufel, F. Aghili, and E. Dupuis, "Task verification facility for the Canadian special purpose dextrous manipulator," *Proc. 1999 IEEE Int. Conf. Robotics and Automation*, pp. 1077-1083, Detroit, Michigan, 1999.